PHYSICAL REVIEW B **92**, 241114(R) (2015)

Glass-ferroic composite caused by the crystallization of ferroic glass

Yuanchao Ji,[1,*] Xiangdong Ding,[1] Dong Wang,[1,†] Kazuhiro Otsuka,[2] and Xiaobing Ren[1,2]

[1]*Frontier Institute of Science and Technology, State Key Laboratory for Mechanical Behaviour of Materials, Xi'an Jiaotong University, Xi'an 710049, China*

[2]*Ferroic Physics Group, National Institute for Materials Science, Tsukuba, 305-0047 Ibaraki, Japan*

(Received 23 February 2015; revised manuscript received 27 June 2015; published 22 December 2015)

We report a glass-ferroic composite (in short "glass-ferroic") in ferroic materials, an analog of the composite of glassy and crystalline phases (glass-crystal composite, e.g., semicrystalline polymer). The formation of glass-ferroic (i.e., the existence of residual ferroic glass) stems from a time-dependent crystallization of the ferroic glass. Moreover, glass-ferroics show two types of transition characteristics depending on the thermal hysteresis of crystallization transition as exemplified in $Ti_{48.7}Ni_{51.3}$ and $Pb_{0.87}La_{0.13}Zr_{0.4}Ti_{0.6}O_3$. Based on experimental results, a generic phase diagram is established to include all ferroic states, i.e., ferroic crystal, ferroic glass, and glass-ferroic. Being the third class of ferroic materials, glass-ferroics may open a new avenue for achieving novel properties and designing ferroic phase-change memory devices.

DOI: 10.1103/PhysRevB.92.241114 PACS number(s): 77.80.Jk, 64.70.dg, 77.80.B−, 81.30.Kf

A crystal or crystalline solid is the archetypal material, which has a long-range ordering of ions, atoms, or molecules through the diffusion. It usually forms from a liquid with cooling (the so-called crystallization transition of liquids). On the other hand, its conjugate state, a structural glass only with a short-range ordering, has also been observed in ceramics, metals, and polymers [1–3]. The crystallization transition of structural glasses yet produces a glass-crystal composite (including glass-ceramic, devitrified metallic glass, and semicrystalline polymer), which can possess superior mechanical, thermal, and optical properties and has also been explored as a phase-change memory device [3–5]. Actually, the glass-crystal can be viewed to be the third class of structural materials (see Table I).

In another large group of ferroic (ferromagnetic/ferroelectric/ferroelastic/multiferroic) solids that are widely used functional and information-storage materials, only the ferroic crystal and ferroic glass have been reported so far (Table I) [6,7]. For these diffusionless systems, the rapid formation of ferroic crystal [6–8] seems to make it impossible to produce the third class—an analogical composite with the glass-crystal, whose formation must rely on an experimental time-scale-dependent transition (in structural materials the formation of glass-crystal involves time-consuming diffusion). In this Rapid Communication, however, we report that the composite of ferroic glass and ferroic phase, which we term "glass-ferroic", can be produced by the time-dependent crystallization transition of ferroic glass upon cooling. This provides evidence for the existing third class of ferroic materials.

We first present the glass-ferroic formation in a solution-treated ferroelastic/martensitic $Ti_{48.7}Ni_{51.3}$ alloy. Upon cooling it undergoes a strain glass transition by exhibiting a frequency dependence of the dip temperature of the storage modulus (inverse of mechanical susceptibility) [Fig. 1(a)] and a frequency dependence of the peak temperature of mechanical loss (tan δ) [Fig. 1(b)]. The frequency dependence of dip temperature (T_g^-) follows the Vogel-Fulcher relation [inset of Fig. 1(a)]. With further cooling, the crystallization or martensitic transition occurs by showing another weak modulus softening [Fig. 1(a)] and mechanical loss peak [Fig. 1(b)]. The decrease in resistivity around the same temperature range further proves the formation of B19' martensite [Fig. 1(c)] because the resistivity of B19' martensite is lower than that of austenite or

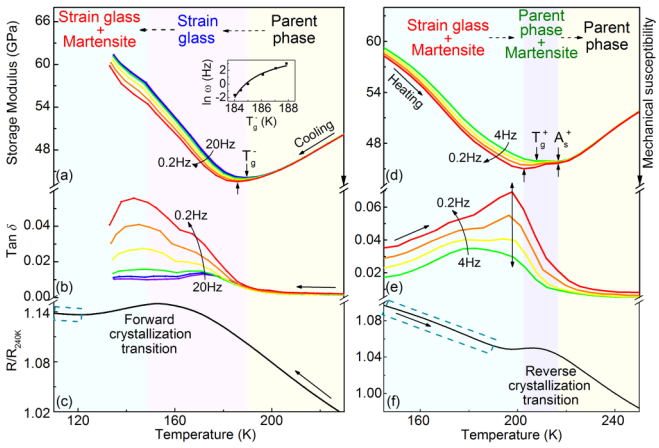

FIG. 1. (Color online) Transition behavior of $Ti_{48.7}Ni_{51.3}$. (a)–(c) Upon cooling the transition sequence, a strain glass transition followed by a forward crystallization (martensitic) transition, is observed. The inset in (a) shows the frequency dependence of the dip temperature of storage modulus (i.e., strain glass transition temperature T_g^-) that follows the Vogel-Fulcher relation [7]. Moreover, the increase in resistivity with decreasing temperature after the martensitic transition [rectangularly marked curve in (c)] indicates the existence of residual strain glass (or strain glass-martensite). (d)–(f) Upon heating an abnormal transition sequence, a reverse strain glass transition (at T_g^+) and a subsequent reverse martensitic transition (at A_s^+), further confirms the strain glass-martensite as the product of forward crystallization transition. It also reveals the irreversibility of crystallization transition: strain glass → martensite upon cooling and martensite → parent phase upon heating. Note the martensitic transition signatures given by the storage modulus and the resistivity are slightly different because of the different temperature measurement designing [18].

*Corresponding author: jiyuanchao@stu.xjtu.edu.cn
†Corresponding author: wang_dong1223@mail.xjtu.edu.cn

 ©2015 American Physical Society

TABLE I. Three classes of transitions and three classes of resulting structural and ferroic materials, where the existence of the third ferroic materials—glass-ferroic was not clear before.

	Structural materials	Ferroic materials
Crystallization transition of liquids	Structural crystal	Ferroic crystal
Glass transition	Structural glass	Ferroic glass
Crystallization transition of glasses	Glass-crystal	Glass-ferroic?

Three classes of transitions are between two of the structural/ferroic liquid, structural/ferroic crystal and structural/ferroic glass. The ferroic case of transition-material correspondence can be further seen in Fig. 5(b).

strain glass [7]. Interestingly, the increase in resistivity after the martensitic transition [Fig. 1(c)] suggests that a residual strain glass (i.e., strain glass-martensite) exists since the resistivity of strain glass increases with decreasing temperature whereas the resistivity of B19' martensite decreases with decreasing temperature [7].

Then upon heating, an abnormal transition behavior was observed. The storage modulus [Fig. 1(d)] and mechanical loss [Fig. 1(e)] curves first show a typical feature of the strain glass transition, a frequency-dependent behavior, which is similar to the one in the cooling process. Upon further heating, the system undergoes another transition, a frequency-independent one, which is a signature of the normal martensitic transition [7,9]. Around the same temperature range, the resistivity curve suggests the occurrence of a reverse B19' martensitic transition [Fig. 1(f)]. Therefore, the heating results do not depict an inverse transition sequence of the cooling process, which are different from the most commonly observed transition characteristics [see an example in Fig. 3(a)] [10–18]. This unique transition sequence challenges the previous understanding of ferroic crystallization transition (see below for details) [10–12,16] and indicates the formation of glass-ferroic.

We further performed the standard zero-field-cooling (ZFC)/field-cooling (FC) measurements to confirm above abnormal transition behavior. The detailed instructions can be found in previous literature [9]. In order to provide a direct comparison, the same experiments were also conducted in a martensitic $Ti_{49}Ni_{51}$ alloy and a strain glass $Ti_{48.5}Ni_{51.5}$ alloy [7]. Figure 2(a) shows ZFC/ZC curves of the $Ti_{48.7}Ni_{51.3}$ alloy. They first exhibit a typical glassy signature of a peak in the ZFC curve and a continuous decrease in the FC curve upon heating as demonstrated in the strain glass $Ti_{48.5}Ni_{51.5}$ alloy [Fig. 2(b)]. With further heating, both ZFC and FC curves show two inflection points that represent the reverse starting and finishing transition temperatures of B19' martensite as demonstrated in the martensitic $Ti_{49}Ni_{51}$ alloy [Fig. 2(c)]. Therefore, these results are fully consistent with Figs. 1(d)–1(f), and we can solidly conclude that: (i) a strain glass-martensite must exist at low temperatures, and (ii) the crystallization transition is irreversible: strain glass → martensite upon cooling and martensite → parent phase upon heating.

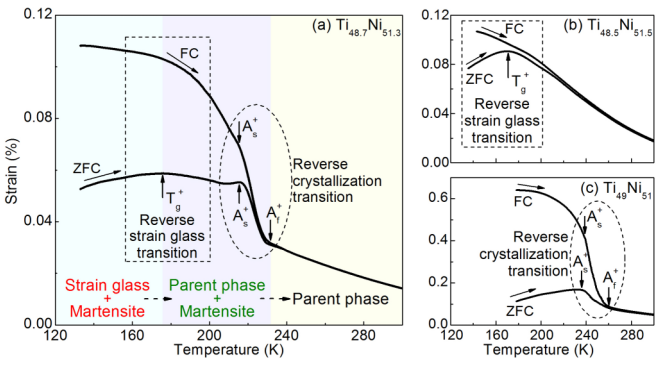

FIG. 2. (Color online) ZFC/FC curves of (a) $Ti_{48.7}Ni_{51.3}$, (b) $Ti_{48.5}Ni_{51.5}$, and (c) $Ti_{49}Ni_{51}$. Through matching with the reverse strain glass transition in $Ti_{48.5}Ni_{51.5}$ and the reverse martensitic transition in $Ti_{49}Ni_{51}$, the transition sequence in $Ti_{48.7}Ni_{51.3}$ is determined to be a reverse strain glass transition and then a reverse martensitic transition. T_g^+, A_s^+, and A_f^+ denote the reverse strain glass transition temperature and the reverse starting and finishing martensitic transition temperatures, respectively.

Next, we reveal the glass-ferroic formation in a ferroelectric $Pb_{0.87}La_{0.13}Zr_{0.4}Ti_{0.6}O_3$ (PLZT) ceramic. Figure 3(a) represents a typical example of the most commonly observed crystallization transition of ferroic glasses [10–18]. Upon cooling, a relaxor transition occurs by exhibiting a frequency-dependent electric susceptibility peak that also follows the Vogel-Fulcher relation [inset of Fig. 3(a)]. With further cooling, the formed relaxor spontaneously transforms into the FE by showing a sharp decrease in electric susceptibility. Upon heating, the transition sequence shows a reversible characteristic [Fig. 3(a)]. Figure 3(b) shows that after the cooling process an external dc electric field (15 kV cm for 48 h at room temperature) was applied to pole the sample. After this treatment, the decreased susceptibility indicates the existence of a residual relaxor (or relaxor-ferroelectric) because of the lower susceptibility of the FE phase than that of the relaxor (see the sharp susceptibility decrease in crystallization transition upon cooling).

Moreover, the heating curves in Fig. 3(b) further clarify the transitions in Fig. 3(a) and confirm the relaxor-ferroelectric formation after the forward crystallization transition. The whole transitions in Fig. 3(a) can be depicted either (i) by PE ↔ relaxor ↔ FE (i.e., a reversible glass transition and a *reversible* crystallization transition) [10–12,16], or (ii) by PE → relaxor → FE upon cooling, FE → PE and relaxor (residual) → PE upon heating (i.e., a reversible glass transition and an *irreversible* crystallization transition). The difference between the two depictions can be simplified to identify the reactant of reverse relaxor transition upon heating, the formed relaxor from the FE or the residual one. After dc polling to eliminate the residual relaxor [Fig. 3(b)], upon heating only a reverse ferroelectric transition, exhibiting a frequency-independent peak of electric susceptibility at T_C^+, was observed. The fact

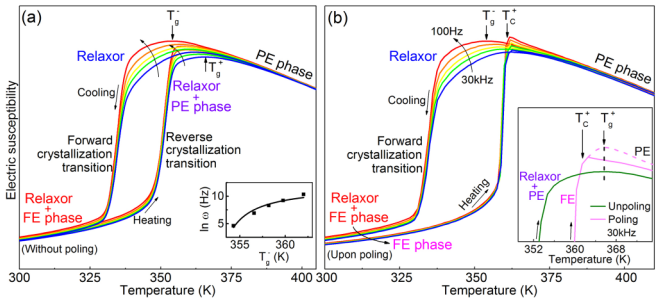

FIG. 3. (Color online) Electric susceptibility of PLZT. (a) Upon cooling PLZT undergoes a relaxor transition and then a forward crystallization transition (i.e., a spontaneous ferroelectric transition), whereas upon heating the reverse crystallization transition occurs from the ferroelectric (FE) component of relaxor-ferroelectric to paraelectric (PE) phase (see below for the reason). The relaxor component is responsible for the reverse relaxor transition. (b) After the dc electric-field poling at room temperature, the susceptibility at low temperatures decreases, indicating the existence of residual relaxor. Upon heating the appearance of reverse ferroelectric transition can be only explained by the irreversible crystallization transition (i.e., FE $\rightarrow$ PE instead of the relaxor), otherwise a peak (reverse relaxor transition) should be found at T_g^+ (as the dashed pink line shows in inset) according to the reversible crystallization transition (i.e., FE $\rightarrow$ relaxor). Accordingly, the reverse relaxor transition in (a) should originate from the residual relaxor, which also indicates that the product of forward crystallization transition is a relaxor-ferroelectric. Note that at low frequencies T_g^+ is lower than T_C^+ (not shown in inset), which cannot be used to exclude the reversible transition scenario.

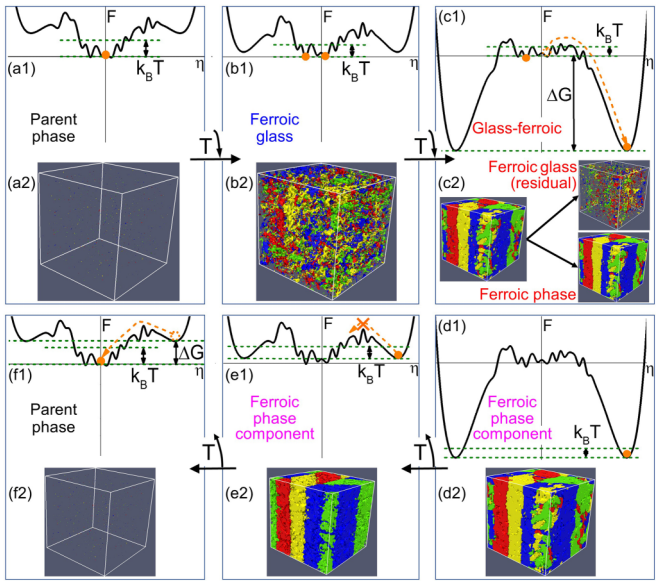

FIG. 4. (Color online) (a1)–(f1) Free-energy landscape and (a2)–(f2) associated microstructure evolution. Upon cooling, the system gradually traps into the minima and forms different configurations (b1) and domains [represented by differently colored regions (b2)]; with further cooling, some configurations and domains transform into the ferroic phase with the help of a large driving force (ΔG), forming a glass-ferroic state (c). Upon heating, the ferroic phase component will not transform into the ferroic glass due to the large energy barrier (e1). When the temperature is high enough, the cooperation between the driving force (ΔG) and the kinetic energy ($k_B T$) leads to a direct transition from the ferroic phase to the parent phase (f). Note (d)–(f) only show the reverse crystallization transition without a reverse glass transition.

that T_C^+ is lower than T_g^+ [inset of Fig. 3(b)] indicates that the crystallization transition is irreversible, otherwise a reverse relaxor transition should appear according to the reversible transition scenario (as the dashed pink line demonstrates). The direct transition from the FE phase to the PE phase without an intermediate relaxor upon heating suggests that: (i) the product of forward crystallization transition is a relaxor-ferroelectric instead of a fully transformed FE phase [12]; (ii) the crystallization transition is irreversible: relaxor $\rightarrow$ FE upon cooling and FE $\rightarrow$ PE upon heating. More discussions on the previous understanding can be seen in Ref. [19].

From the results of $Ti_{48.7}Ni_{51.3}$ and PLZT, it can be concluded that the crystallization transition of ferroic glasses produces the glass-ferroic. It originates from a time-dependent crystallization process, which can be understood in the context of a classical free-energy landscape containing multiple minima (basins) separated by local barriers [1,20,21]. The associated microstructure evolution upon continuous cooling and heating was simulated by the phase field modeling [19]. Upon cooling, the system, which in the parent phase can continuously explore different configurations [Fig. 4(a1)], will gradually trap in specific basins. Because of the low kinetic energy ($k_B T$), some local barriers caused by disorder (e.g., point defects [7,20,21] and nanosized precipitates [9]) cannot be overcome, thereby leading to "frozen" configurations (a glass state) [Fig. 4(b1)]. The heterogeneity of disorder in the glass state [1] gives rise to a distribution of the time-dependent formation of the stable ferroic phase (i.e., crystallization). Upon further cooling, the driving force increases, and thus some configurations with low local barriers [Fig. 4(c1)] or domains with low disorder [Fig. 4(c2)] can undergo a crystallization transition in a much shorter time. Yet others with high disorder cannot crystallize immediately because they are trapped among high local barriers and need sufficient time to overcome their local barriers, thereby keeping a glass state. This time dependence explains why the crystallization transition of ferroic glass produces the glass-ferroic instead of the ferroic crystal.

Upon heating, the ferroic phase component first keeps the stability due to a high-energy barrier [Fig. 4(e1)]. When it transforms, the driving force from the ferroic phase to the parent phase is larger than the local one to ferroic glass. Meanwhile, the kinetic energy is also high to overcome local barriers [Fig. 4(f1)]. Therefore, the increase in both driving force and kinetic energy upon heating (i.e., a cooperation relationship) supports the transition directly from the ferroic phase to the parent phase [Fig. 4(f)], which is different from the situation upon cooling that the driving force increases whereas the kinetic energy decreases (i.e., a competition relationship) [Fig. 4(c)].

Next, we will explain why the glass-ferroic shows two types of transition characteristics as demonstrated in $Ti_{48.7}Ni_{51.3}$ and PLZT. The difference involving the sequence between the reverse glass transition (at T_g^+) and the reverse crystallization ("melting") transition (at T_m) (i.e., $T_g^+ < T_m$ or $T_g^+ > T_m$) can

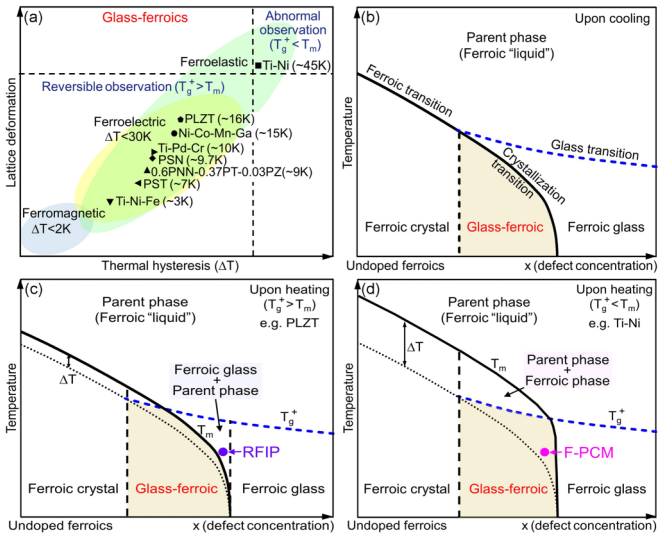

FIG. 5. (Color online) (a) Rough classification of glass-ferroics based on the thermal hysteresis and lattice deformation of crystallization transitions: the abnormal observation only occurs when the thermal hysteresis (or lattice deformation) is large enough, such as in $Ti_{48.7}Ni_{51.3}$, whereas the reversible (normal) one occurs when the thermal hysteresis is much smaller. The data of Ti-Ni and PLZT are from the present study, Ni-Co-Mn-Ga ($Ni_{45}Co_{10}Mn_{20}Ga_{25}$) is from Ref. [15], Ti-Pd-Cr ($Ti_{50}Pd_{40}Cr_{10}$) is from Ref. [17], PSN ($PbSc_{0.5}Nb_{0.5}O_3$) is from Ref. [14], 0.6PNN-0.37PT-0.03PZ ($0.6PbNi_{1/3}Nb_{2/3}O_3$-$0.37PbTiO_3$-$0.03PbZrO_3$) is from Ref. [11], PST ($PbSc_{0.5}Ta_{0.5}O_3$) is from Ref. [13], and the others are from Ref. [22]. (b)–(d) Generic temperature vs defect-concentration ferroic phase diagram upon cooling, upon heating ($T_g^+ > T_m$), and upon heating ($T_g^+ < T_m$), respectively. T_g^+ and T_m denote the reverse glass transition and reverse crystallization (melting) transition temperatures. Three classes of ferroic states, i.e., ferroic crystal, glass-ferroic, and ferroic glass, are produced by three corresponding classes of transitions, i.e., ferroic transition, crystallization transition, and glass transition, respectively. Besides four states in (b), the phase diagram upon heating of (c) and (d) shows an additional composite state depending on T_g^+ and T_m. The dotted line, purple and pink dots in (c) and (d) represent the ferroic and crystallization transition curves upon cooling, the state which has the potential application of reversible field-induced properties (RFIP, e.g., large electrostriction with low hysteresis [24]) and ferroelectric phase-change memory (F-PCM) devices (similar to PCM in chalcogenide glass [5]), respectively.

be attributed to the scale of thermal hysteresis (the difference between forward and reverse transition temperatures) of crystallization transitions because of little thermal hysteresis of glass transitions [7,9]. Thermal hysteresis is known to strongly depend on the stability of the ferroic phase: The more stable a ferroic phase is, the larger the thermal hysteresis is, and the higher T_m is [22,23]. Moreover, the stability can be further estimated by the magnitude of lattice deformation since the entropy change is proportional: (i) to the lattice deformation for ferroelectric and ferromagnetic systems [22] and (ii) to the square of the lattice deformation for ferroelastic systems [23]. For example, a large lattice deformation (~10%) of $Ti_{48.7}Ni_{51.3}$ [23] explains a large hysteresis (~45 K) whereas a small lattice deformation (<2%) of PLZT [10] gives rise to a small hysteresis (~16 K). Therefore, the reason why all previously reported transition characteristics of glass-ferroics appear reversibly ($T_g^+ > T_m$) is due to the small thermal hysteresis (or lattice deformation) [Fig. 5(a)]. The abnormal observation ($T_g^+ < T_m$) only occurs when the thermal hysteresis is large enough, such as in $Ti_{48.7}Ni_{51.3}$. Note that the transition sequence in structural glasses ($T_g^+ < T_m$) can also be understood under the same criterion, a large thermal hysteresis (i.e., the large difference between T_m and $T_{crystallization}$).

The finding of glass-ferroic may lead to many important consequences. First, as the third ferroic state besides ferroic crystal and ferroic glass (Table I), the glass-ferroic universally exists in the phase diagram [Figs. 5(b)–5(d)], which is a fundamental improvement over previously reported phase diagrams [7,18,25] that show two ferroic states corresponding to three classes of phase transitions. Second, glass-ferroics may open a new field to develop functional materials and devices as glass-crystals have proved in structural materials [3,4]. For example, the large reversible field-induced physical property [in the purple dot of Fig. 5(c)] can be expected, and this is confirmed by our ongoing study [24]. Moreover, the F-PCM device [in the pink dot of Fig. 5(d), given that it is at room temperature] can be designed: By applying a heat pulse, it can be switched between a relaxor state (through a natural cooling after applying intense pulse of heat to increase temperature over T_m) and a ferroelectric state (through a time-induced crystallization of the relaxor after applying a lower-intensity heat pulse of longer duration below T_m), thereby changing dielectric and optical (e.g., birefringent) properties and allowing the storage of information. The same diffusionless transformation process with ferroelectric random access memory (F-RAM) [26] indicates some expected advantages of F-PCM, such as low power usage, fast read/write performance, and overcoming the degradation problem of traditional PCM. In addition, the PCM principle of F-PCM could also overcome the destructive reading problem of F-RAM [26]. In short, the phase diagram in Fig. 5 will be a fundamental guiding for where to find glass-ferroics and how to design glass-ferroic properties.

The work was supported by the National Basic Research Program of China (Grants No. 2012CB619401 and No. 2014CB644003), the National Natural Science Foundation of China (Grants No. 51171140, No. 51231008, No. 51320105014, No. 51321003, No. 51201125, and No. 51431007), and the Program for Changjiang Scholars and Innovative Research Team in University (Grant No. IRT13034).

[1] K. Binder and W. Kob, *Glassy Materials and Disordered Solids: An Introduction to Their Statistical Mechanics* (World Scientific, Singapore, 2005).

[2] T. Egami, in *Bulk Metallic Glasses*, edited by M. Miller and P. Liaw (Springer, New York, 2007).

[3] K. Kelton and A. L. Greer, *Nucleation in Condensed Matter: Applications in Materials and Biology* (Pergamon, Oxford, UK, 2010).

[4] W. Holand and G. H. Beall, *Glass-Ceramic Technology*, 2nd ed. (Wiley, Hoboken, NJ, 2012).

[5] M. Wuttig and N. Yamada, Nature Mater. **6**, 824 (2007).
[6] V. K. Wadhawan, *Introduction to Ferroic Materials* (Gordon and Breach, Amsterdam, 2000).
[7] X. Ren, Phys. Status Solidi B **251**, 1982 (2014); in *Disorder and Strain-Induced Complexity in Functional Materials*, edited by T. Kakeshita, T. Fukuda, A. Saxena, and A. Planes (Springer, Berlin, 2012), Vol. 148.
[8] A. Grigoriev, D. H. Do, D. M. Kim, C. B. Eom, B. Adams, E. M. Dufresne, and P. G. Evans, Phys. Rev. Lett. **96**, 187601 (2006).
[9] Y. Ji, X. Ding, T. Lookman, K. Otsuka, and X. Ren, Phys. Rev. B **87**, 104110 (2013).
[10] X. Dai, A. DiGiovanni, and D. Viehland, J. Appl. Phys. **74**, 3399 (1993); X. Dai, Z. Xu, and D. Viehland, J. Am. Ceram. Soc. **79**, 1957 (1996); (T_{rn} and T_{nr} were used to denote the transition temperature between the relaxor and the normal ferroelectric phase).
[11] M. Yoon and H. M. Jang, J. Appl. Phys. **77**, 3991 (1995).
[12] G. Deng, A. Ding, G. Li, X. Zheng, W. Cheng, P. Qiu, and Q. Yin, J. Appl. Phys. **98**, 094103 (2005).
[13] F. Chu, N. Setter, and A. K. Tagantsev, J. Appl. Phys. **74**, 5129 (1993).
[14] F. Chu, I. M. Reaney, and N. Setter, J. Appl. Phys. **77**, 1671 (1995).
[15] Y. Wang, C. Huang, H. Wu, J. Gao, S. Yang, D. Wang, X. Ding, X. Song, and X. Ren, Appl. Phys. Lett. **102**, 141909 (2013).
[16] O. Bidault, E. Husson, and A. Morell, J. Appl. Phys. **82**, 5674 (1997). (T_{R-nFE} and T_{nFE-R} were used to denote the transition temperature between the relaxor and the normal ferroelectric phases).
[17] D. Xue, Y. Zhou, X. Ding, Y. Wang, J. Zhang, J. Sun, and X. Ren, Phys. Status Solidi B **251**, 2019 (2014).
[18] Y. Yao, Z. Sun, Y. Ji, Y. Yang, X. Tan, and X. Ren, Sci. Technol. Adv. Mater. **14**, 035008 (2013).
[19] See Supplemental Material at http://link.aps.org/supplemental/10.1103/PhysRevB.92.241114 for details of experimental methods and discussions on the previous understanding of crystallization transition.
[20] Y. Ji, D. Wang, X. Ding, K. Otsuka, and X. Ren, Phys. Rev. Lett. **114**, 055701 (2015).
[21] Z. Sun, D. Xue, H. Wu, Y. Ji, X. Ding, and X. Ren, Appl. Phys. Lett. **102**, 222907 (2013).
[22] S. Yang, X. Ren, and X. Song, Phys. Rev. B **78**, 174427 (2008).
[23] K. Otsuka and X. Ren, Prog. Mater. Sci. **50**, 511 (2005).
[24] M. Fang, Y. Ji, and X. Ren (to be published).
[25] X. Dai, Z. Xu, and D. Viehland, J. Appl. Phys. **79**, 1021 (1996).
[26] R. Guo, L. You, Y. Zhou, Z. S. Lim, X. Zou, L. Chen, R. Ramesh, and J. L. Wang, Nat. Commun. **4**, 1990 (2013).